Supramolecular Lattice Deformation and Exciton Trapping in Nanotubular J-Aggregates

*Megan D. Klein[†], Katherine E. Shulenberger[‡], Ulugbek Barotov, Tara Šverko, Moungi G. Bawendi**

Department of Chemistry, Massachusetts Institute of Technology, 77 Massachusetts Avenue, Cambridge, Massachusetts 02139, United States

KEYWORDS Excitons, J-Aggregates, Exciton Trapping, Photobrightening, Lattice Deformation, C8S3

ABSTRACT Interactions between excitons and molecular vibrational modes limit the extent of exciton delocalization and rate of energy transport in organic molecular aggregates, diminishing their performance in many optical device applications. This coupling leads to exciton self-trapping and subsequently changes their emission behavior. Certain amphiphilic cyanine dyes form nanotubular aggregates that demonstrate high exciton transport rates and show no such coupling between excitons and molecular vibrational modes. However, under sustained illumination these aggregates undergo photobrightening (PB) and can show a doubling in quantum yield. We investigate this reversible PB process through spectral- and time-resolved photoluminescence (PL) measurements under low illumination intensities. We observe lengthening exciton lifetimes with no corresponding spectral change. Furthermore, wide-angle X-ray scattering measurements show

a change in the aggregate structure following PB. We propose a model of PB through large polaron formation, leading to trapping or shielding of these long coherence length excitons through interactions with supramolecular vibrations, rather than the intramolecular vibrations typically observed in other aggregates. These excitons are then less able to access non-radiative recombination sites, which leads to the observed increase in quantum yield. The lattice deformations persist after emission and accumulate over time, resulting in brightening of the aggregate under sustained illumination. We support this model through temperature-, color-, and matrix-dependent photoluminescence measurements and show that the model correctly predicts the changes observed upon addition of a FRET quencher. Finally, we demonstrate control over PB behavior through rigidification of the aggregate with a silica shell, potentially enabling the development of long term-photobrightened devices utilizing molecular aggregates with significantly higher photoluminescence quantum yields.

INTRODUCTION

Molecular aggregates of organic dyes have been the focus of photophysical research for a number of years due to their unique optical properties and potential applications ranging from sensitizers, to luminescent concentrators, and optoelectronics.[1–8] The electronic structure of these self-assembled systems strongly depends on the alignment of the individual monomers' transition dipoles. If the transition dipoles interact constructively it results in J-aggregates, with characteristic, red-shifted and narrowed absorption and emission bands.[9,10] If the transition dipoles interact destructively, however it leads to the counterpart H-aggregates with a blue-shifted absorption and emission.[11] The nature of whether this interaction is constructive or destructive comes entirely from the orientation of the monomers in the self-assembly of the aggregate.[12] The

red-shifted absorption and emission of J-aggregates results from their bright band edge state, and the narrowing of their linewidths occurs due to motional narrowing dependent on the coherence length of the aggregate.[13,14] Because of the direct influence of monomer alignment on coupling, the structural homogeneity of self-assembly can strongly affect the energetic landscape of the aggregate – aggregates with high energetic disorder will show lower exciton delocalization than aggregates with minimal energetic disorder. This decrease in delocalization will lengthen the radiative lifetime of the aggregate, broaden the linewidth, and minimize the red-shift.[13,15] While these effects are significant, structural disorder is not the only factor that can alter the exciton dynamics of J-aggregate species however; processes such as exciton trapping also play a large role in changing the observed behavior.

Exciton self-trapping occurs in many types of molecular aggregates when an exciton couples to an intramolecular vibrational mode of the monomer (such as a C=C stretch) and results in a lower energy state.[16] This trapping process is observed in many aggregates with short coherence lengths and can be identified by the emergence of emission that is further redshifted by the energy of the vibrational mode and a spectrally dependent lifetime, with a lower decay towards the red edge.[17] In some cases, the formation of an exciton can lead to a deformation in the aggregate structure itself, coupling the intermolecular lattice vibrations to the exciton. If this coupling is sufficiently strong it can also lead to a self-trapped exciton, or small polaron, such as the case in the work of Sorokin *et al*. on layered films of J-aggregates.[17,18] When the coupling is below a critical value, the result is the formation of a large polaron.[19,20] Most J-aggregates that have been studied in this regard though demonstrate *intra*molecular polaron formation. The few which demonstrate *inter*molecular interactions couple to the lattice vibrations sufficiently strongly to localize the exciton onto only one or two monomers.[21–23] All of these J-aggregate systems have

relatively short coherence lengths however, as there are few known aggregates with a low enough disorder to yield long coherence lengths from tens to hundreds of monomers. One such J-aggregate is that of the dye monomer C8S3.

Several previous studies have investigated the properties of J-aggregates formed by the Cy3 derivative, 3,3'-bis(3-sulfopropyl)-5,5',6,6'-tetrachloro-1,1'-dioctylbenzimidacarbocyanine, also known as C8S3. The amphiphilic nature of this dye leads to self-assembly into double-walled nanotubular J-aggregates, with the hydrophobic octyl chain on the inside of the bilayer, and the hydrophilic sulfonate groups oriented outwards.[24–26] These nanotubules have outer diameters of 12.4 ± 1.1 nm, and can range from hundreds of nanometers to several microns in length.[27] Moreover, C8S3 aggregates demonstrate low energetic disorder and no vibrational side bands.[28,29] The aggregates show strong absorption and emission, and are estimated to have exciton delocalization lengths on the order of hundreds of molecules.[30] Measurements of exciton transport rates in this system have given values ranging from 120-5500 nm^2ps^{-1}.[27,31] While this range is very broad, it suggests fast exciton diffusion across long distances. This high rate of energy transport has been shown to enhance the effectiveness of these aggregates when acting as antennas in light concentrating or photosensitizing applications.[32]

Aggregates of C8S3 have also demonstrated emergent photo-behavior under sustained excitation.[33] Under sufficiently high excitation densities, the aggregates photodarken (PD) rapidly, with some subsequent long-term recovery. Previous work has attributed this to monomer sites being removed from the aggregate coupling, possibly due to charging from free carrier separation.[33] Additionally, initial photobrightening (PB) was observed wherein the quantum yield of the aggregate will increase briefly under excitation and then diminish during PD. This is of particular note since PB behavior has rarely been observed in fluorescent organic systems.[34]

Previous studies of PB have primarily occurred in inorganic semiconductor nanocrystals. The reported brightening mechanism in these systems involves the filling of long-lived trap states under sustained excitation, leading to saturation of those states and an increase in steady-state fluorescence of the nanocrystals.[35,36] Determining whether a similar mechanism applies to PB in molecular aggregates as well requires a more thorough study of the changes in excitonic behavior in these systems.

In this work we utilized a variety of spectroscopic techniques to investigate the excitonic and structural nature of the PB mechanism in C8S3 J-aggregates, including time-resolved photoluminescence (PL) measurements, temperature- and color-dependent excitation, and wide-angle X-ray scattering (WAXS). We propose a model of supramolecular lattice deformation to explain the observed changes during PB and show that this model not only agrees with the original measurements, but also explains the results seen upon addition of a Förster resonance energy transfer (FRET) acceptor to act as a quencher of the aggregate system. Finally, we also demonstrate control over the recovery of the photobrightened state through rigidification of the aggregate structure.

METHODS

J-Aggregate Preparation. J-Aggregate samples were prepared from a 2.92 mM stock solution of C8S3 monomer (FEW Chemicals S0440) in methanol (Fisher Chemical, >99.8%). Glass vials were soaked in purified water (MilliQ, 20 Ω) prior to use in order to prevent bundling of C8S3 aggregates. In a pre-soaked vial, 130 uL of C8S3 stock solution were added to 500 uL purified water (MilliQ, 20Ω) to induce aggregation. The resultant 0.60 mM solution was mixed by gently inverting to avoid disrupting the aggregate structure, then left between 2 h and overnight to ensure

complete aggregate formation. Following aggregate formation, the samples were then diluted with a further 500uL of purified water for a final concentration of 0.34 mM C8S3. For solid state samples, 200uL of the 0.60 mM solution was taken and diluted with 200uL of a trehalose/sucrose solution: 2 g trehalose (Sigma Aldrich T9449-100G), 2 g sucrose (Sigma Aldrich), 2 mL water. 115 uL of this solution was then deposited on a demountable quartz cuvette (0.2 mm pathlength, Starna Cells 20/C-Q-0.2) and dried overnight in a desiccator covered with aluminum foil to prevent light exposure. Quenching experiments were performed by incorporating a concentrated solution of Atto 633 dye (Sigma Aldrich 18620-1MG) in water prior to mixing with the trehalose/sucrose solution in order to obtain the desired concentration ratio. Liquid samples were prepared in a glovebag under a nitrogen atmosphere, with water that had been sparged under nitrogen for 15 mins. These samples were encapsulated in 0.2 mm pathlength glass capillaries (Vitrocom, #3520) and sealed at both ends with Cryto-Seal.

UV-Vis Absorption spectra were collected using a Cary 5000 spectrophotometer (Agilent) with the samples prepared in the aforementioned 0.2 mm demountable quartz cuvettes.

TEM To prepare the silica coated J-aggregates for cryo-TEM, 3 uL of the sample was dropped on a lacey copper grid coated with a continuous carbon film (Lacey Formvar Stabilized with Carbon, 200 mesh). Excess solution was removed from the grid by blotting the sample using Gatan Cryo Plunge III. The sample was then quickly plunged into liquid ethane to flash freeze and stabilize the silica coated J-aggregates in aqueous solution at approximately -175 °C. The grid was mounted on a Gatan 626 single tilt cryo-holder equipped in the microscope column. The sample and the holder tip were cooled by liquid nitrogen during transfer into the microscope and subsequent imaging. The sample was imaged using JEOL 2100 FEG microscope under minimal dose, which was essential to prevent J-aggregate degradation under the electron beam. The microscope was

operated at 200 kV and a magnification in the range of 10,000X – 60,000X. All images were collected using Gatan 2000 x 2000 UltraScan CCD camera.

Lifetime Measurements Samples were excited with the 404 nm doubled output of a Ti:Sapph oscillator (78 MHz, Coherent Mira 900-F) focused through a lens (f = 20 cm). Excitation powers were measured on a photodiode power meter (Thorlabs S121C). Emission was collected with a pair of 2 in. parabolic mirrors and focused into a spectrometer (Bruker 250IS) with a 300 groove/mm grating. The spectrally dispersed output from the spectrometer was then directed into a streak camera (Hamamatsu C5680) with an attached syncroscan sweep unit (Hamamatsu M5675). Streak images were collected with 200 ms integration time and 100 integrations. Image analysis and emission decay trace fitting were performed using a homebuilt Matlab library.

Photobrightening Experiments for PB were performed on the streak camera setup described above. For solid state samples, the focused laser spot could be used to induce PB, with a sequence of streak images being collected over the course of the experiment. For solution samples, a 530 nm LED was used to illuminate a wide area of the sample to avoid having to worry about diffusion in and out of the PB region (1 mW/cm^2, Thorlabs M530L4). Temperature-dependent PB measurements were performed by placing the sample in a transfer line cryostat (Janis ST-100) and cooling with either liquid helium or liquid nitrogen. Recovery measurements were obtained by turning off the illumination source and leaving the samples in the dark for the specified amount of time, then measuring the emission decay again.

Color-Dependent Photobrightening The streak camera setup used for lifetime measurements was modified by adding a 50:50 beamsplitter into the excitation path. A second laser source for PB was then aligned co-linear to the beam from the Mira laser, to ensure that lifetime

measurements and PB both occurred at the same spot. The two PB laser sources used were 1) CW 532nm Ventus and 2) CW 400nm Melles Griot. Spot sizes were measured using a razor blade and a micrometer in order to calculate excitation densities. The Mira beam was blocked for most of the experiment to prevent additional PB due to the pulsed source and only unblocked for brief periods to collect emission decay traces. To ensure this small amount of illumination required to measure the lifetimes was not responsible for the PB effects observed, a control experiment was also performed with only the brief illumination from the Mira and no second PB illumination source.

WAXS Measurements X-ray measurements were performed on a SAXSLAB Ganesha instrument (Xenocs) with a Cu X-ray source (Rigaku 002 microfocus) and collected on a Pilatus 300K detector (Dectris). Solution samples were prepared in quartz capillaries (1.5 mm, Hampton Research HR6-148) sealed with wax. Sugar matrix samples were suspended in a thin layer on a small ring washer to provide a substrate-free path for measurement. Scattering traces were worked up in the SASview software package.

Rigidified Aggregates Silica-coated C8S3 J-aggregates were prepared following a slightly modified literature method.[37] Inside a glove-bag, 1:49 v/v methanol solutions of (3-aminopropyl)triethoxysilane (APTES) and tetraethoxysilane (TEOS) were prepared. Subsequently, 4.5 uL APTES solution and 34 uL TEOS solution were added to a vial containing 500 uL milli-Q water. The resulting solution was quickly stirred and 130 uL stock C8S3 solution (2.92 mM in methanol) was added immediately. The sample was covered with aluminum foil and stored in the dark. After 24 hours, additional 500 uL water was added to the silica coated J-aggregate solution.

RESULTS AND DISCUSSION

SAMPLE PREPARATION AND CHARACTERIZATION

We prepared aggregates of C8S3 dye through the previously reported alcoholic route[24] to yield self-assembled double-walled nanotubules, depicted in **Figure 1a**. Cryogenic transmission electron microscopy (Cryo-TEM) shows the morphology of these aggregates (**Figure 1b**). The alcoholic preparation ensures there is no formation of the alternate, bundled morphology of C8S3 aggregates. Following previous work in our group, we were able to stabilize the aggregates against photo-oxidation through incorporation into a dried sucrose-trehalose sugar matrix.[27] These nanotubular structures demonstrate J-aggregate behavior, with an absorption red-shift of 68 and 78 nm to the outer and inner wall peaks, respectively, and narrowing of the absorption peak compared to the C8S3 monomer, as seen in **Figure 1c**.

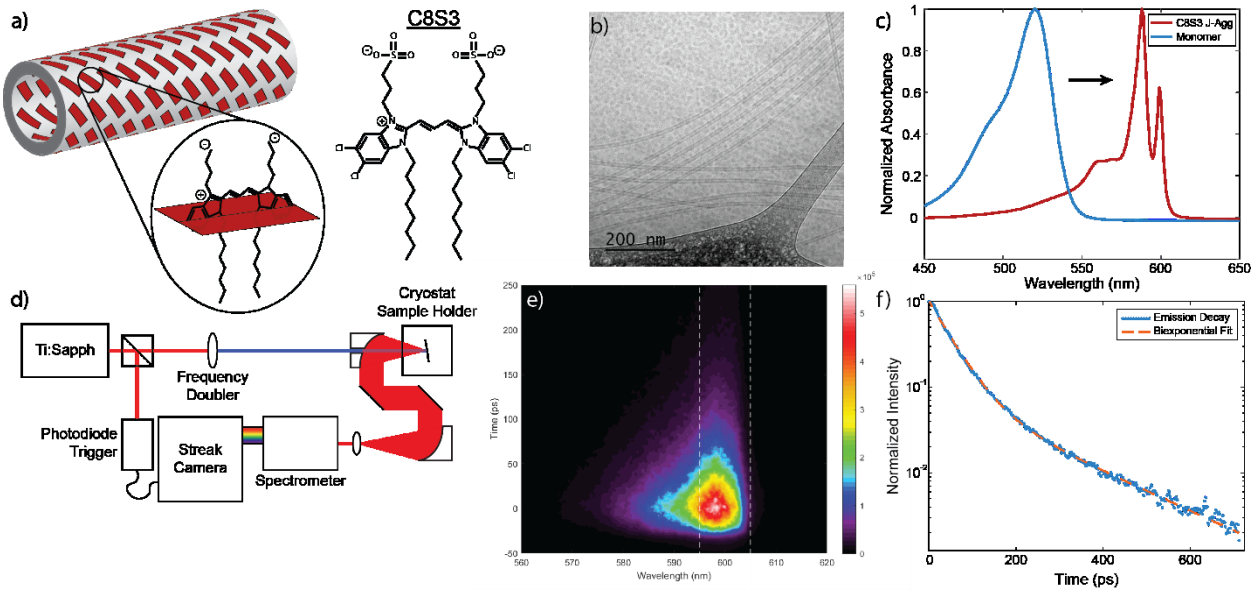

Figure 1. a) Cartoon depicting double-walled nanotubular structure of C8S3 aggregates (Inset, simplified diagram of C8S3 orientation in aggregate structure. Hydrophilic moieties point outward into solution while hydrophobic octyl chains point inward. Heteroatoms omitted for visual clarity) Right, structure of C8S3. **b)** Cryo-TEM micrograph of C8S3 J-aggregates. Scale bar is 200 nm. **c)** Normalized absorption spectra of C8S3 monomer (blue) with a maximum at 520 nm and aggregate (red) with outer wall peak at 588 nm and inner wall peak at 598 nm. **d)** Schematic of streak camera setup used to measure time- and wavelength-resolved PL. **e)** Example of streak image from C8S3 J-aggregate emission. Dashed vertical lines denote wavelength range selected to isolate IW emission, 595-600 nm. Lifetime traces were collected by integrating across these wavelengths. **f)** PL decay of C8S3 IW emission (blue), with biexponential fit (orange).

We performed further characterization of the emission dynamics of these aggregates using the streak camera setup shown in **Figure 1d**. The spectral and temporal resolution of this setup allowed us to follow the dynamics of a single peak in the aggregate emission spectrum. For the purpose of this study, we focused on the emission from the inner wall (IW) of the aggregates, extracting dynamics from the 595-600 nm wavelength range (**Figure 1e**). We confine our studies to the IW because it is the primary emission path for the aggregates due to its lower energy transition, as well as being more isolated from the environment compared to the outer wall. Under ambient conditions, we observe that the emission from these C8S3 J-aggregates decays biexponentially, which we fit and extract rate constants of 2.17×10^{-2} ps^{-1} and 5.3×10^{-3} ps^{-1} (**Figure 1f**), with 95% confidence intervals ($CI_{0.95}$) of $[2.13 \times 10^{-2},\ 2.21 \times 10^{-2}]$ ps^{-1} and $[5.2 \times 10^{-3},\ 5.4 \times 10^{-3}]$ ps^{-1}, respectively. Note that while the lifetime decays of both walls of the aggregate are similar, shown in **Figure S1**, the biexponential behavior is not due to the double-walled nature of the aggregates. In **Figure S2** we demonstrate that the emission from the IW still follows a biexponential decay even in the absence of the outer wall. While previous work has also reported this biexponential decay, the minor component has typically been considered insignificant and disregarded.[33] However, through fitting to a biexponential curve, we estimate the percentage of emission from the long lifetime component to be 28% under ambient conditions with a $CI_{0.95}$ of [26.8-28.5]%, which represents a sizeable contribution to the overall emission and therefore cannot be neglected.

PHOTOBRIGHTENING BEHAVIOR AND STRUCTURAL EFFECTS

Upon continued exposure to light, C8S3 aggregates have been observed to exhibit both PB and PD.[33] At low illumination intensities, continued photo-exposure over the course of minutes to hours results in roughly a factor of 2 increase in the relative quantum yield (QY) of these

aggregates, with no observable spectral changes in the emission (**Figure 2a**), or the absorption (**Fig. S3**). As the illumination intensity increases, PD behavior becomes more and more pronounced, and the aggregates demonstrate slight brightening followed by significant darkening. Previous studies ascribed PB behavior to annealing of static energetic disorder among the aggregate sites.[33] However, that work primarily focused on PD, and any photobrightening effects were observed under higher excitation fluences than used here, likely convolving PB with more significant PD effects. In this work we isolate solely PB behavior by utilizing low illumination intensities to minimize PD, and therefore distinguish the spectroscopic signature of these two processes.

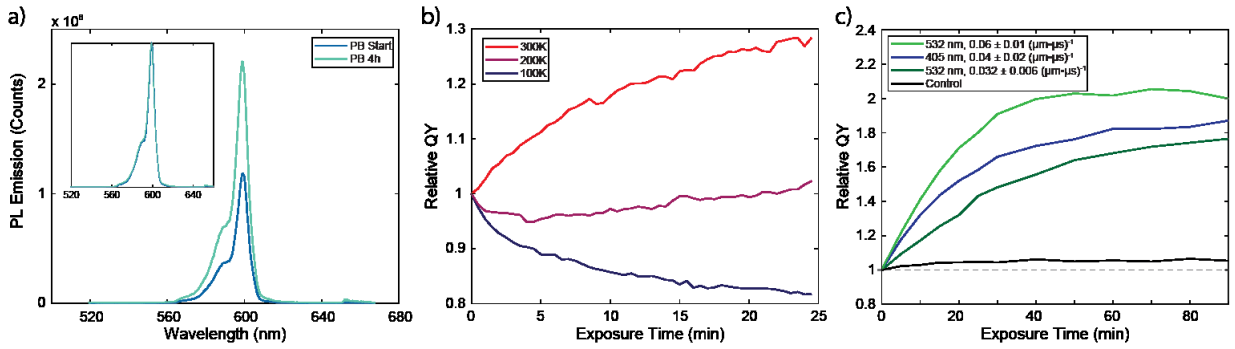

Figure 2. a) Emission spectra of C8S3 J-aggregates before PB (dark blue) and after 4 hours of illumination (light blue). The integrated area of the emission spectrum increases by a factor of 1.9 during the experiment. Inset shows normalized emission spectra, demonstrating no observable spectral changes. **b)** Temperature-dependent PB measurements showing relative quantum yield over the course of a PB series run at 300 K (red), 200 K (purple), and 100 K (blue). **c)** Color-dependent PB measurements comparing continuous wave excitation at 532nm (light green, dark green) and 405 nm (blue). Excitation densities are given in terms of excitations per μm per μs. The control (black) shows the change in relative QY from the brief illumination of pulsed 405 nm light used to measure at each time point.

To determine the effect of thermal energy on PB, we monitored the emission quantum yield under sustained illumination as a function of temperature. Photobrightening is greatly reduced at lower temperatures and at 100K no PB is observed, instead we see only slight darkening (**Figure 2b**). This temperature-dependence of PB suggests that ambient thermal energy is necessary for the brightening mechanism. Without enough thermal energy, sustained illumination only results in PD. Previous work has demonstrated, however, that the quantum yield of the aggregates decreases

as the temperature is raised as a result of higher disorder limiting the extent of delocalization.[29] As such, thermal energy cannot be the driving mechanism behind PB. As demonstrated by these results, thermal energy plays a necessary role in the photobrightening mechanism, but ambient thermal effects alone are not sufficient to cause photobrightening.

With this observation that thermal energy is necessary for PB, we then tested whether local heating from the absorption of above band-edge photons was the driving force behind photobrightening. We investigated this by studying the dependence of PB behavior on the wavelength of illumination. The IW aggregate peak emits at 600 nm, so we chose to compare the PB behavior under 404 nm and 532 nm illumination, corresponding to an excess energy above the band-edge of 1.00 eV and 0.26 eV per photon, respectively. **Figure 2c** shows the results of the color-dependent illumination experiments. Using the spot size and aggregate absorption spectrum, we were able to closely match excitation densities between the wavelengths to directly compare the effect of above band-edge excess energy on a per-excitation basis. Due to the uncertainty in these values from both measuring the spot size and the extremely low absorption of the aggregates at 404 nm however, we ran the experiment at the minimum and maximum of the expected range of matching densities of 532 nm illumination to better compare to the 404 nm excitation. We observe extremely similar PB behavior independent of the wavelength of illumination. If there were a color-dependence to PB, we would expect it to dramatically vary the brightening behavior due to the nearly four-fold increase in above-bandgap energy between the 532 nm and 404 nm photons. Instead, this result suggests that a change in the excess photon energy above the bandgap has minimal impact on brightening. The lack of excitation wavelength dependence in combination with the previous measurement showing ambient thermal energy is necessary for PB implies that this brightening process requires a high occupancy of thermal modes in the aggregate itself, but

that local heating from excitation with above band-edge photons is not the cause of PB behavior. The necessity of ambient thermal energy and the lack of effect of local heating on PB suggests that there may be a relation between the brightening process and the structural behavior of the aggregate lattice and environment.

For this reason, we turn to investigating the impact of the surrounding environment and look at matrix effects on the behavior of the aggregates. Photobrightening occurs on the timescale of minutes to hours and, upon stopping the illumination, can exhibit recovery on similarly long timescales. The kinetics of photobrightening are highly dependent on the supporting matrix of the aggregate. While we have previously shown that a dried sugar matrix prevents photo-oxidation of the aggregates and enables measurements at cryogenic temperatures, it is also possible to prepare C8S3 J-aggregates under air-free conditions to stably measure them in solution. **Figure 3a** shows a comparison between PB and recovery behavior of C8S3 J-aggregates in a dried sugar matrix, the corresponding sugar solution before drying, and in pure water. These three different conditions differ predominantly in the viscosity of the matrix, and therefore the mobility of the atomic components of the aggregates. Even without considering the PB effects, the dynamics of the intrinsic PL decay vary strongly between different supporting matrices. The PL decay traces can be fit to biexponential functions with the parameters shown in **Table 1**. The aggregates in water and sugar solution both show similar biexponential fit parameters, but when the aggregate is embedded in a solid-state matrix, the initial fast decay accelerates.

Table 1. Extracted parameters from biexponential fits of matrix-dependent PL decay traces. The lower and upper bounds of the $CI_{0.95}$ are given in the sub- and superscript, respectively.

Matrix	c_1	k_1 (ps^{-1})	Area 1 (c_1/k_1)	c_2	k_2 (ps^{-1})	Area 2 (c_2/k_2)
Dried Sugar	$0.93^{0.95}_{0.91}$	$2.17^{2.21}_{2.13} \cdot 10^{-2}$	$43.0^{43.6}_{42.3}$	$0.088^{0.093}_{0.082}$	$5.3^{5.4}_{5.2} \cdot 10^{-3}$	$16.5^{17.0}_{15.9}$
Sugar Solution	$0.84^{0.85}_{0.83}$	$1.39^{1.42}_{1.36} \cdot 10^{-2}$	60^{62}_{59}	$0.11^{0.12}_{0.10}$	$5.2^{5.4}_{5.0} \cdot 10^{-3}$	21^{23}_{19}
Water	$0.85^{0.87}_{0.84}$	$1.29^{1.32}_{1.26} \cdot 10^{-2}$	66^{69}_{64}	$0.13^{0.15}_{0.11}$	$5.3^{5.5}_{5.0} \cdot 10^{-3}$	25^{28}_{23}

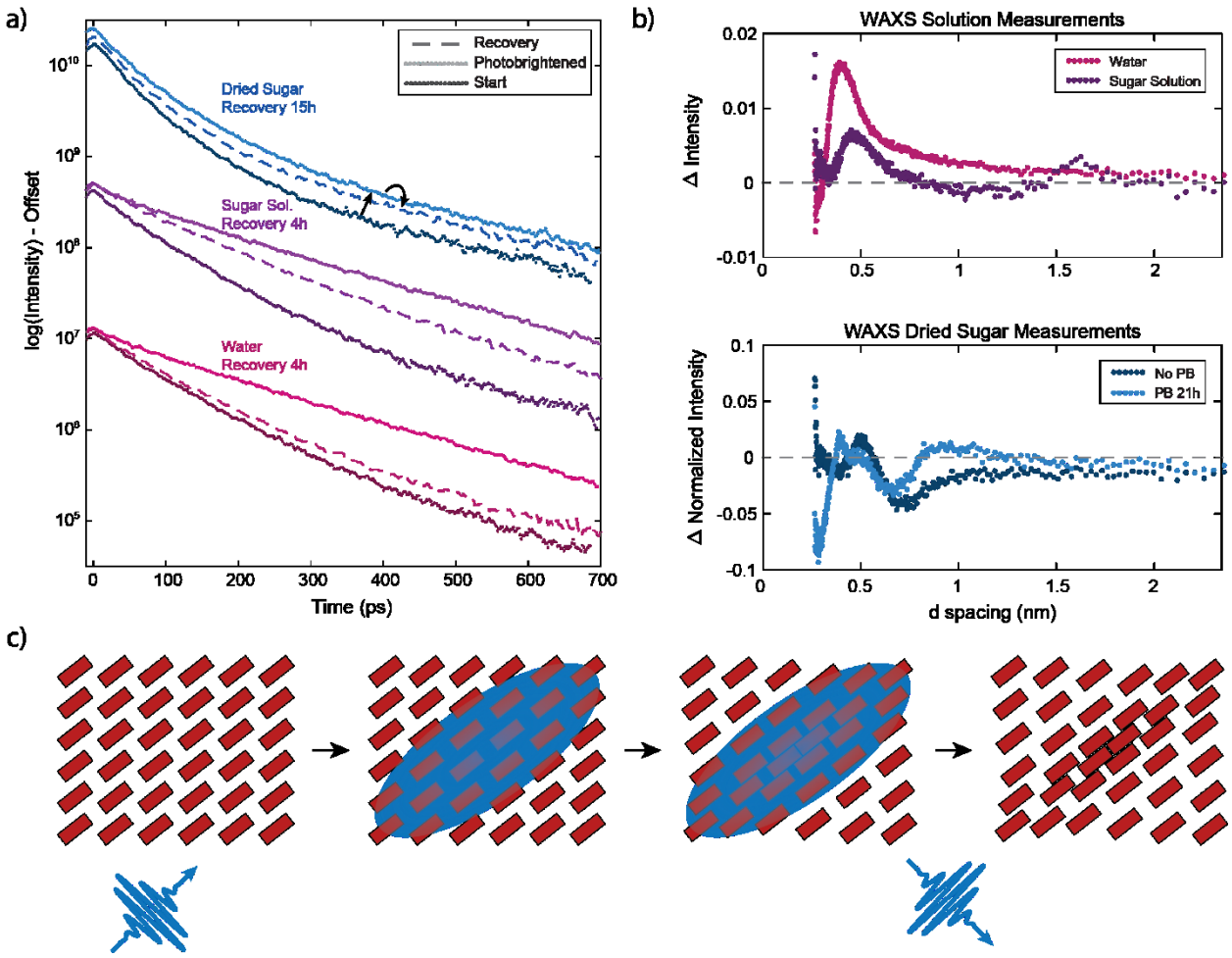

Figure 3. a) Lifetime traces of C8S3 J-aggregates before PB (dark circles), after 3.5 hours of illumination (light circles), and after recovery (dashed line). Comparison shows different PB behavior depending on the supporting matrix of the aggregates in dried sugar (blue), sugar solution (purple), and water (red). **b)** Top: WAXS measurements showing structural difference of C8S3 J-aggregates in water (red), and sugar solution (purple). Bottom: Normalized WAXS measurements demonstrating structural change between C8S3 J-aggregates in dried sugar without PB (dark blue) and after 21 hours of PB (light blue) **c)** Schematic depicting hypothesized deformation of supramolecular lattice in response to photoexcitation, resulting in biexponential lifetimes and photobrightening.

Figure 3a also shows that PB recovery behavior varies with the supporting matrix. Over the course of a 3-hour illumination, aggregates in water were observed to increase in relative QY by a factor of 2.1±0.4, while in sugar solution that factor was 2.3±0.4, and in dried sugar it was only a factor of 1.6±0.2. Once the illumination was halted, aggregates in water exhibit near-complete PB recovery over 3.5 hours, aggregates in sugar solution recovered partially over the same time, and in the dried sugar matrix almost no recovery was observed even over 18 hours. As the viscosity of the matrix increases, the aggregate is slower to undergo and recover from any PB

changes. This further supports the hypothesis that any PB changes involve a structural change in the aggregate. A more viscous solution, or even a rigid, dried matrix slows the reversal of these changes and results in a photobrightened state that persists over many hours.

To probe structural changes more directly, we turned to wide angle X-ray scattering measurements (WAXS) to investigate the C8S3 J-aggregates in different matrices and following PB. A comparison of the diffraction patterns in **Figure 3b** shows a notable shift in the d-spacing of the primary aggregate peak, from 0.40 nm in water, to 0.46 nm in the sugar solution, and 0.50 nm in the dried sugar matrix. While detailed structural information is difficult to extract from this data due to the exceedingly low concentration of aggregates and the lack of strongly scattering atoms, the supporting matrix still has a clear effect on the structure of the aggregates. Given the strong dependence of excitonic behavior on lattice geometry in molecular aggregates, this would then lead to changes in the aggregate emission dynamics, which is what we observe.[12] Because of the slow recovery of photobrightened C8S3 J-aggregates in a dried sugar matrix, we were able to illuminate the sample overnight and then measure the diffraction pattern of the photobrightened structure to compare. This result is also shown in **Figure 3b**. Notably, there are significant structural differences between the aggregate peak without PB and the aggregate peak with PB, in particular the diminishment of the 0.50 nm peak and the appearance of a narrow peak at 0.40 nm. This evidence directly supports a structural change occurring as a result of photo-exposure. Although the decreasing length scale observed suggests that the monomers are shifted closer together upon PB, this does not necessarily correspond to stronger coupling between monomers because the J- or H-like character of a 2D aggregate is strongly dependent on the angle and slip distance between monomers and the exact geometry of the lattice arrangement.[38] The increase in lifetime observed with this photobrightened state suggests that the deformation actually results in

lower J-like coupling between dye molecules. Furthermore, the observation of this change over macro timescales means that the structural changes persist after emission of the photon and accumulate over time, leading to PB effects on the timesecale of minutes to hours.

The pieces of evidence demonstrated above, namely 1) the necessity of ambient thermal energy, 2) the lack of effect from local heating due to above band-edge excitation, 3) the dependence of PB behavior on the viscosity and rigidity of the supporting matrix, and 4) the direct observation of structural changes through WAXS, together suggest that a deformation of the overall aggregate lattice occurs upon sustained illumination. This proposed mechanism is illustrated in **Figure 3c**. The J-aggregate lattice consists of a brickwork-like assembly, where each brick is a monomer of the anionic C8S3 dye. Upon absorption of a photon, the resultant exciton is delocalized across a large number of these monomer sites. Given sufficient ambient thermal energy, the supramolecular lattice then deforms in response to this exciton. The result is an exciton that is either shielded or trapped in the aggregate. This exciton then emits with a longer lifetime, as it is less able to access non-radiative recombination sites that are available for freely diffusing excitons, resulting in a higher QY for the trapped or shielded excitons. Due to the high activation barrier for lattice reorganization, the deformed site is slow to revert when the exciton is no longer present, and these deformed sites accumulate over time resulting in the observed PB effects under sustained illumination.

EXCITON TRAPPING

To further investigate the mechanism of PB, we studied the aggregate emission dynamics, focusing particularly on the biexponential rate constants and integrated area fractions of each component. Because the emission decay trace of these aggregates can be fit to a biexponential

function, we obtain a fit of the form $I(t) = c_k e^{-kt} + c_j e^{-jt}$. Here, $I(t)$ is the observed intensity as a function of time, c_k and c_j are prefactors to each exponential, and k and j are the underlying rate constants of each component. We can extract further information from these fit parameters as well with the integrated areas, $A_k = kc_1$ and $A_j = jc_2$. To determine how the structural changes occurring during PB affect the photophysical behavior of the aggregates, we examine the dynamics of the ensemble aggregate over the course of PB. **Figure 4** shows the overall changes between the initial decay trace and the decay following four hours of PB. Of note is the slowing of the early component and the increasing fraction of light emitted from the late component. Based on these qualitative changes, we construct a kinetic model of differential equations that describe transfer from a free population (η) to a trapped/shielded population (ξ) with rate k_{trap}, where each population has additional non-radiative (k_{nr}, j_{nr} for the free and trapped states, respectively) and radiative decay (k_r, j_r again for the free and trapped states, respectively) pathways. The cartoon in **Fig. 4b** depicts the relevant populations and rates. The system of equations is as follows:

$$\frac{\partial[\eta]}{\partial t} = -\big(k_r + k_{nr} + k_{trap}\big)[\eta]$$

$$\frac{\partial[\xi]}{\partial t} = k_{trap}[\eta] - (j_r + j_{nr})[\xi]$$

$$\frac{\partial P}{\partial t} = k_r[\eta] + j_r[\xi]$$

Note that $\frac{\partial P}{\partial t}$ is the rate of photon emission, which is the quantity measured in our photoluminescence experiment. Solving this system as described in section S-IV of the SI leads to the following equation describing the emission behavior:

$$\frac{\partial P}{\partial t} = \left(k_r \eta_0 - j_r \frac{\eta_0 k_{trap}}{k_{tot} - j_{tot}}\right) e^{-k_{tot} t} + \left(j_r \xi_0 + j_r \frac{\eta_0 k_{trap}}{k_{tot} - j_{tot}}\right) e^{-j_{tot} t}$$

Where η_0 and ξ_0 are the initially excited populations in the free and trapped/shielded state, respectively. The sum of rates from each state are simplified as $k_{tot} = k_r + k_{nr} + k_{trap}$, and $j_{tot} = j_r + j_{nr}$.

With this model we can now look more closely at how the parameters extracted from biexponential fits of the lifetimes vary as a function of illumination time (**Figure 4c-e**). The rate constant of the early component drops from 2.17×10^{-2} ps^{-1} ($[2.13 \times 10^{-2}, 2.21 \times 10^{-2}]$ ps^{-1}) initially to 1.31×10^{-2} ps^{-1} ($[1.27 \times 10^{-2}, 1.36 \times 10^{-2}]$ ps^{-1}) following four hours of exposure, while the rate constant of the late component remains constant over the entire four hours. From the total integrated areas, we observed the early component increasing by a factor of 1.3 while the late component increases in area by a factor of 3.5, even becoming the majority component of the emission towards the end of the four hours. Previous explanations of PB behavior have suggested

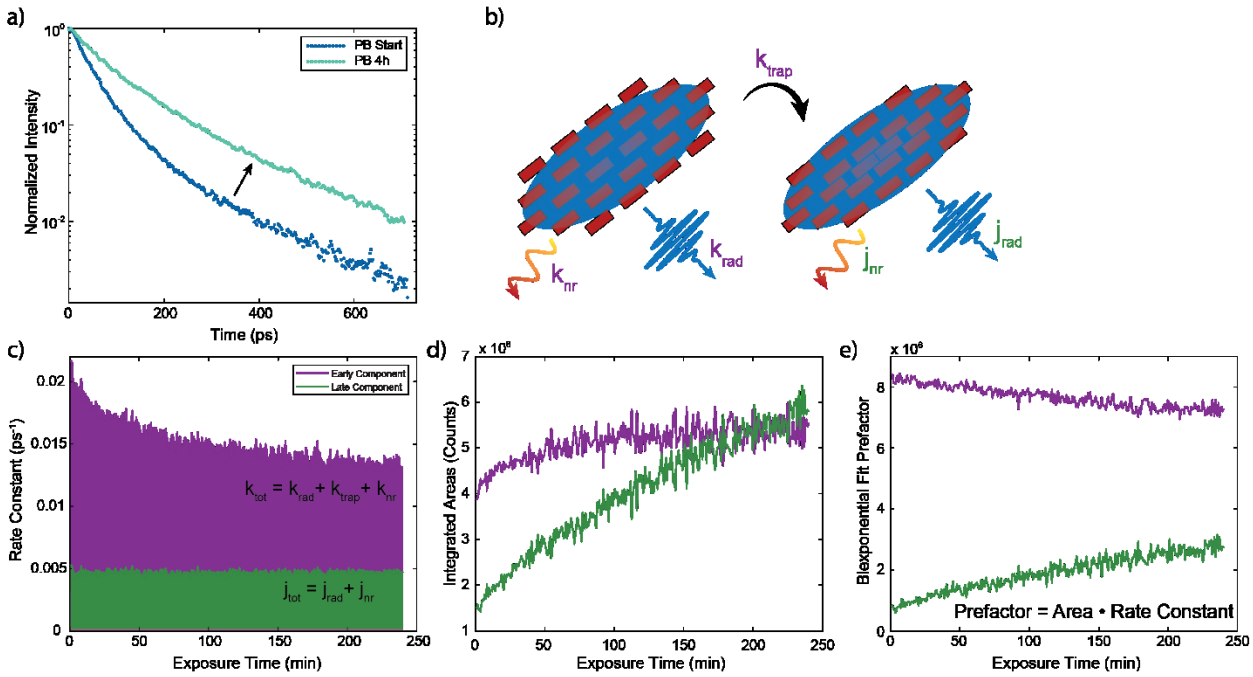

Figure 4. a) Lifetime traces of C8S3 J-aggregates before PB (dark blue) and after 4 hours of illumination (light blue) showing the change in emission dynamics. **b)** Schematic of the decay pathways and rates from the free and trapped states used in the differential equation model. **c)** The change in rate constants of the early (purple) and late (green) lifetime components extracted from biexponential fits as a function of exposure time, demonstrating the decrease in the early component during PB. **d)** The change in integrated area of the early (purple) and late (green) lifetime components during PB. **e)** Changes in the early (purple) and late (green) prefactors of the biexponential fit during PB.

an annealing of non-radiative rates leading to an increased QY.[33] The decreasing value we measure of k_{tot} supports the idea of annealing non-radiative pathways, however it does not decrease sufficiently to explain the nearly four-fold increase in emission from the late component. In addition to the decreasing k_{nr}, there must be an increase in a trapping rate, k_{trap}, transferring the population into a longer lived, higher QY trapped state. The decreasing non-radiative rate would result in an overall increase of emission, and the increasing trapping rate directly explains the increase in late component emission with no change to the late component rate constant. Given that the increased emission during PB is primarily a result of the slow, trapped population it is likely that the trapped excitons have a higher QY than the free excitons. In combination with the longer lifetime of the trapped state, this would suggest that the trapped excitons experience less non-radiative recombination, possibly due to being slower to diffuse along the aggregate and

access non-radiative recombination sites. In that case, this increase in the trapped population would explain the dramatic brightening that is observed under sustained illumination.

We have established that PB results in direct structural changes in the aggregate and an increase of a longer lifetime component with higher PLQY. As a final confirmation of this mechanism, we test the nature of the trap state through a fluorescence quenching experiment. If the J-aggregate lattice is deforming around the exciton, then we expect it to either trap the exciton by modifying the coupling of nearby monomers and limiting delocalization, or to shield the exciton by deforming the charged lattice around the carriers, or both. To measure this effect, we incorporated a second dye to act as a FRET acceptor, quenching emission from the C8S3 aggregate. Atto 633 (**Figure 5a**) has an absorption peak at 630 nm but emits at 651 nm - well separated from any aggregate emission. Moreover, this dye is positively charged and expected to associate with the negatively charged C8S3 J-aggregate. By varying the concentration of Atto dye we can construct a series of samples with varying FRET transfer rates. From the absorption spectra we can see that the addition of the Atto dye does not affect the structure of the C8S3 aggregate (**Figure 5b**). We can then measure the emission decay of the J-aggregate peak to observe how the dynamics change with increasing quencher concentration. **Figure 5c** shows the reduced emission and change in decay traces as the molar ratio of quencher:C8S3 monomer goes from 0 to 0.067, and **Figure 5d-f** shows the change in extracted parameters from biexponential fits. In particular, the rate constant of the early component increases dramatically from $2.38 \pm 0.09 \times 10^{-2}$ ps^{-1} to $4.2 \pm 0.2 \times 10^{-2}$ ps^{-1}, while the rate constant of the late component does not appear to change significantly.

As these experiments were done in a dried sugar matrix, the path length at the measured spot could vary slightly from sample to sample due to drying artifacts. Because of this, we compare

the prefactor ratio and integrated area fraction rather than absolute numbers to avoid discrepancies due to path length differences. We observe an increase in the early:late prefactor ratio from 25 ± 1 to 45 ± 4 with increasing quencher concentration, while no significant change occurs in the integrated area fractions, despite the overall emission area decreasing. This means the emission from both the early and late component decreases equally, however we only observe a change in the rate constant of the early component. This can be readily explained if there is a free exciton population capable of rapidly transferring to the FRET quencher, and a second exciton population that cannot access the quencher – either because it is trapped and cannot diffuse freely to find the quencher, or because it is shielded and the resultant decrease in effective oscillator strength limits the FRET transfer rate. At higher concentrations, the quencher will rapidly deplete the population of free excitons before they can emit or trap. This will lead to the observed change in the early component rate constant, while leaving the second rate constant unaffected. The behavior of the fit prefactors and areas is more complicated however, as it will not follow a simple branching ratio model. For more detail, we include the discussion of this behavior in Section S-V and **Fig. S4** of the SI. We observe that by this model, an increase in k_{nr} due to quenching will lead to a corresponding increase in the prefactor ratio. However, the change in the non-radiative rate will not result in a similar increase in the area ratio, as it may be offset by any initial exciton population absorbed into the trapped state, ξ_0. This matches what we observe upon incorporation of the quencher with the aggregates.

With the model that we have constructed from observations about PB and structural behavior of the aggregate also explaining the changes seen upon the addition of a quencher, this strongly supports the idea that exciting C8S3 J-aggregates leads to a population of free excitons that can become trapped or shielded in deformed sites of the supramolecular lattice. These sites then accumulate throughout the duration of excitation and result in PB. This is in stark contrast to the behavior of many other types of J-aggregates, where exciton self-trapping occurs through *intra*-molecular vibrations, coupling to vibrational modes of the individual dye monomers.[16] Given the much longer coherence length of excitons in C8S3 J-aggregates[30], it is a plausible extension that the delocalized excitons interact with *inter*-molecular motions over larger length scales throughout the lattice. While this type of deformation has been observed prior in a small number of aggregates, it typically results from strong coupling to the lattice modes, resulting in a highly localized self-

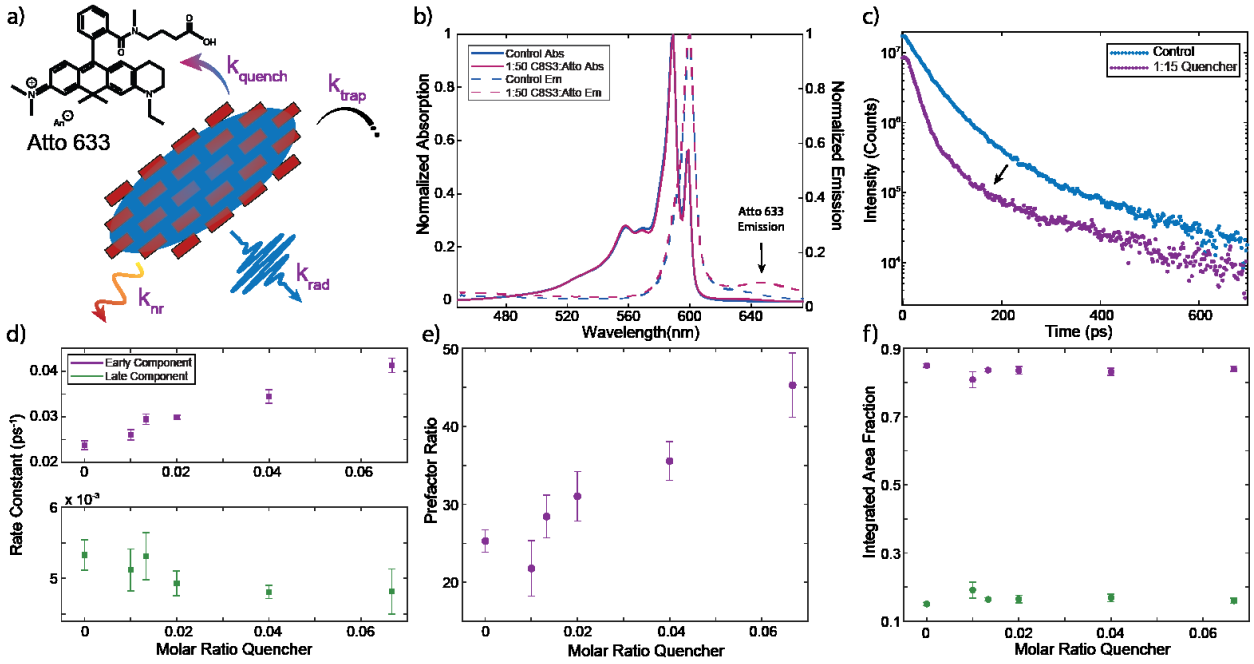

Figure 5. a) Addition of Atto 633 dye as a FRET acceptor provides another decay pathway for freely diffusing excitons in the J-aggregate. **b)** Absorption (solid) and emission (dashed) spectra of a control C8S3 aggregate sample (blue) and a 1:50 molar ratio of C8S3:Atto 633 (magenta). **c)** The change in lifetime decay between the control (blue) and a 1:15 molar ratio of C8S3:Atto 633 (purple). **d)** The change in rate constants of the early (purple) and late (green) lifetime components with increasing Atto 633 concentration. **e)** Changes in the ratio of early:late prefactors extracted from the biexponential fit as a function of Atto 633 concentration. **f)** Changes in the integrated area fraction of the early and late lifetime components as a function of Atto 633 concentration.

trapped exciton.[17–19] In **Figure S5** we show an analysis of the Urbach edge of the C8S3 aggregate absorption to find an estimate of the coupling constant. We obtain a principally coupled phonon mode energy of $312 \pm 8\ cm^{-1}$ and a coupling constant on the order of $g = 0.37 \pm 0.07$. This is below the threshold $g_c = 0.87$ for exciton self-trapping in a square lattice and instead suggests coupling to form a large polaron, which agrees with the behavior we observe for PB.[20] Finally, the value for $\hbar\omega$ closely matches the 315 cm^{-1} observed as a coupling mode of the C8S3 aggregates by Pandya *et al.*, who assigned the mode to a supramolecular lattice vibration in the aggregate.[39] These results from analyzing the Urbach edge therefore further support the proposed model of large polaron formation leading to PB in C8S3 J-aggregates.

Previous literature reports of exciton self-trapping in J-aggregates through intramolecular vibrations have shown that the resulting emission is lengthened in lifetime, red-shifted from the original J-band peak, and demonstrates a lower quantum yield.[17,40] In comparison, the emission that we observe from photobrightened C8S3 aggregates is also lengthened in lifetime, but has no resolvable change in energy from the non-brightened emission spectrum in the course of brightening. A potential explanation for this arises from the fact that the band levels in a J-aggregate are strongly dependent on the aggregate geometry and the alignment of the monomer transition dipoles[12]. Particularly in higher-dimensional aggregates, the precise arrangement of angles and slip distances plays a large role in the nature of J- versus H- coupling between monomers.[38] This means the change in lattice energy due to exciton shielding could be offset by a change in coupling between monomers the new geometry. The shielded exciton is then less able to access potential non-radiative recombination sites and results in brightening of the aggregate. The detailed interaction between intermolecular motion or deformation in J-aggregates and its effect on coupling has been as of yet unexplored, however. A further analysis could reveal insight

into excitonic behavior that arises in molecular aggregates with long coherence lengths that are affected by these intermolecular vibrations and exciton trapping or shielding.

This trapping or shielding behavior also offers an explanation for the wide range of exciton transport lengths measured in C8S3 J-aggregates. Clark *et al*. measured exciton diffusion through confocal microscopy and observed a diffusion constant of 120 nm^2ps^{-1}.[31] Using power-dependent measurements, Caram *et al*. investigated exciton diffusion via exciton-exciton annihilation and reported a diffusion constant of 5500 nm^2ps^{-1}.[27] Our observation of significant photoinduced trapping or shielding in these aggregates means that the underlying diffusive behavior of excitons will change significantly throughout the duration of optical experiments due to the accumulation of these sites.[41] Any attempts to measure transport rates in these aggregates must be done incredibly carefully with respect to excitation powers and illumination times to prevent PB or PD from impacting the observed behavior.

RIGIDIFICATION THROUGH SILICA COATING

As well as providing fundamental insight into a rarely studied trapping mechanism in J-aggregates, this research also provides an avenue towards potential control over the photophysical properties of the aggregates. To investigate a possible approach to controlling aggregate behavior, we looked to coat the C8S3 aggregates with a shell to rigidify their structure. Notably, there have been multiple reports in the literature of forming nanocomposites from these aggregates with a silica shell.[37,42] We proceeded to synthesize silica-coated C8S3 J-aggregates following a modified procedure from Qiao *et al*.[37] TEM micrographs of these aggregates show nanotubes surrounded by a 2.3 nm silica shell (**Figure 6a**). The silica coating has minimal effect on the absorption and emission spectra, (**Figure 6b**), but we would expect it to provide a rigid support for the overall

lattice of the aggregate and influence the ability to recover from deformation. To test this, we performed PB recovery measurements on the silica-coated aggregates in water, shown in (**Figure 6c**). We observe a similar amount of brightening to the uncoated aggregates in water, but a significant difference in their recovery following 4 hours, recovering by only 29% compared to the 61% observed for the uncoated water sample. We conclude that the silica shell rigidifies the aggregate structure in an analogous way to the stability of the solid-state dried sugar matrix. This

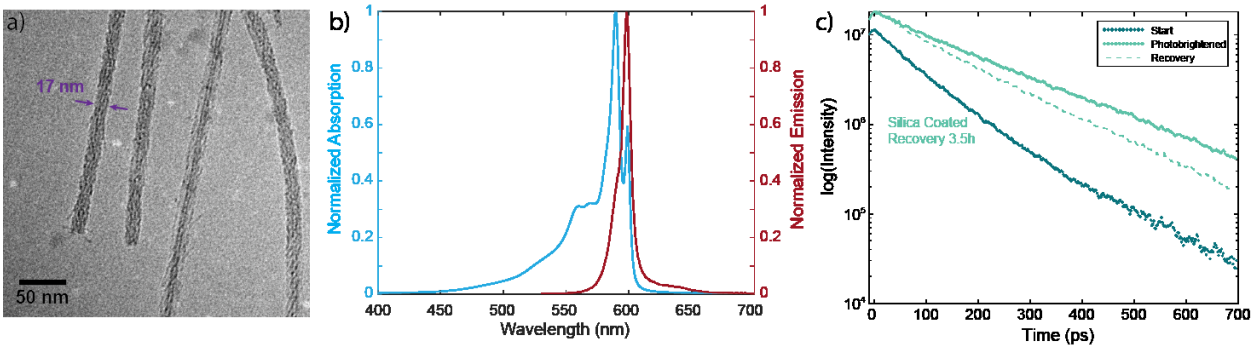

Figure 6. a) TEM micrograph of silica-coated C8S3 J-aggregates shows diameters of 17 nm, compared to the 12.4 nm of bare aggregates, suggesting a silica shell thickness of 2.3 nm. **b)** Absorption (blue) and emission (red) spectra of a silica-coated aggregate sample showing the J-aggregate spectrum is minimally affected by the silica coating process. **c)** Lifetime traces of silica-coated aggregate before (teal circles) and after (aqua circles) 3.5 hours of photobrightening, as well as 3.5 hours of recovery (dashed line).

rigidity limits the ability of the aggregate to recover from deformation and preserves the photobrightened state. In optical device applications of aggregates, this approach could provide a means to increase the QY of the aggregates and improve their device performance by effectively "pre-photobrightening" aggregates in such a way that they will remain brightened over a long term. Future explorations could investigate alternate architectures for rigidifying the aggregate structure and better preserving the photobrightened state.

CONCLUSIONS

We have investigated the mechanism of photobrightening in C8S3 J-aggregates through studying excitonic and structural behavior under sustained illumination. Using thorough emission dynamics

studies as well as direct structural measurements *via* WAXS, we propose a mechanism involving the deformation of the supramolecular aggregate lattice around an exciton to form a large polaron, resulting in a trapped or shielded exciton that limits access to non-radiative recombination sites and thus leads to an increase in the quantum yield and a lengthened fluorescence lifetime. This deformation requires sufficient thermal energy present in the aggregate but is not a local heating effect and specifically requires excitation to occur. This mechanism of trapping is distinct from typical self-trapping in molecular aggregates, which involves strong coupling to a molecular vibrational mode and leads to distinct red-shifted side bands and lower quantum yields. Photobrightening of C8S3 aggregates occurs as these lattice deformation sites accumulate over the aggregate and the overall emission increases. It is also accompanied by an annealing of non-radiative pathways of the free exciton population, preventing depletion of excitons before they can reach the trapped or shielded state. We have further demonstrated that the supporting matrix of the aggregate has a significant effect on its ability to recover from photobrightening. We utilize this matrix effect to show that rigid silica shell coatings provide a pathway to control the photophysical behavior of the aggregates and limit their recovery from photobrightening. This opens the way to potential engineering approaches to control aggregate emission for device applications through long-term photobrightening of aggregates to increasing their quantum yield. Finally, these results also lay the groundwork for more fundamental studies of aggregate behavior, such as exploring the nature of whether deformation of the aggregate lattice specifically results in a trapped exciton or a shielded exciton, as well as investigating the mechanism behind the lower QY of free excitons in the aggregates.

ASSOCIATED CONTENT

Supporting Information. The supporting information is available free of charge on the ACS Publications website.

Comparison between inner and outer walls, isolated inner wall J-aggregate, PB absorption behavior, kinetic model discussion, quenching kinetics discussion, and Urbach edge analysis (PDF)

AUTHOR INFORMATION

Corresponding Author

*Email: mgb@mit.edu. Phone: 617-253-9796.

ORCID

Megan D. Klein: 0000-0002-0758-4294

Katherine E. Shulenberger: 0000-0002-5464-101X

Ulugbek Barotov: 0000-0002-8931-9127

Tara Šverko: 0000-0002-2046-9151

Moungi G. Bawendi: 0000-0003-2220-4365

Present Addresses

† Department of Chemistry, University of Washington, Seattle, Washington 98195, United States
‡ Department of Chemistry, University of Colorado Boulder, Boulder, Colorado 80309, United States

Author Contributions

The manuscript was written through contributions of all authors. All authors have given approval to the final version of the manuscript.

Notes

The authors declare no competing financial interest.

Acknowledgments

M.D.K. (lead author, data collection, analysis – including interpretation and software development) was supported by a National Science Foundation Graduate Research Fellowship Under Grant No. 1122374, as well as a grant from the Institute for Soldier Nanotechnologies No. W911NF-18-2-0048. K.E.S. (analysis and interpretation) was supported by the U.S. Department of Energy, Office of Science, Basic Energy Sciences under Award No. DE-FG02-07ER46454. U.B. (TEM images, silica-coated aggregate synthesis) was supported by the National Science Foundation under Grant No. CHE-2108357. T.Š. (PB recovery analysis) was supported by the U.S. Department of Energy, Office of Science, Basic Energy Sciences under Award No. DE-SC0021650. The WAXS data presented in this work made use of the MRSEC Shared Experimental Facilities at MIT, supported by the National Science Foundation under award number DMR-1419807. We would like to acknowledge Dr. Charles Settens in the MIT-MRSEC X-ray Diffraction Shared Experimental Facility for his guidance on WAXS data collection and workup. We would also like to acknowledge Dr. Francesca Freyria for her cryo-TEM work in collecting the micrograph of uncoated C8S3 J-Aggregates.

REFERENCES

(1) Lanzafame, J. M.; Muenter, A. A.; Brumbaugh, D. V. The Effect of J-Aggregate Size on Photoinduced Charge Transfer Processes for Dye-Sensitized Silver Halides. *Chem. Phys.* **1996**, *210*, 79–89.

(2) Walker, B. J.; Bulović, V.; Bawendi, M. G. Quantum Dot/J-Aggregate Blended Films for Light Harvesting and Energy Transfer. *Nano Lett.* **2010**, *10*, 3995–3999.

(3) Freyria, F. S.; Cordero, J. M.; Caram, J. R.; Doria, S.; Dodin, A.; Chen, Y.; Willard, A. P.; Bawendi, M. G. Near-Infrared Quantum Dot Emission Enhanced by Stabilized Self-Assembled J-Aggregate Antennas. *Nano Lett.* **2017**, *17*, 7665–7674.

(4) Ishimoto, C.; Tomimuro, H.; Seto, J. Multiple Wavelength Optical Recording Using Cyanine Dye J Aggregates in Langmuir-Blodgett Films. *Appl. Phys. Lett.* **1986**, *49*, 1677–1679.

(5) Wang, C.; Weiss, E. A. Sub-Nanosecond Resonance Energy Transfer in the Near-Infrared within Self-Assembled Conjugates of PbS Quantum Dots and Cyanine Dye J-Aggregates. *J. Am. Chem. Soc.* **2016**, *138*, 9557–9564.

(6) Wang, C.; Weiss, E. A. Accelerating FRET between Near-Infrared Emitting Quantum Dots Using a Molecular J-Aggregate as an Exciton Bridge. *Nano Lett.* **2017**, *17*, 5666–5671.

(7) Ribierre, J. C.; Sato, M.; Ishizuka, A.; Tanaka, T.; Watanabe, S.; Matsumoto, M.; Matsumoto, S.; Uchiyama, M.; Aoyama, T. Organic Field-Effect Transistors Based on J-Aggregate Thin Films of a Bisazomethine Dye. *Org. Electron.* **2012**, *13*, 999–1003.

(8) Hecht, M.; Schlossarek, T.; Ghosh, S.; Tsutsui, Y.; Schmiedel, A.; Holzapfel, M.; Stolte, M.; Lambert, C.; Seki, S.; Lehmann, M.; et al. Nanoscale Columnar Bundles Based on Multistranded Core–Shell Liquid Crystals of Perylene Bisimide J-Aggregate Donor–Acceptor Dyads for Photoconductivity Devices with Enhanced Performance Through Macroscopic Alignment. *ACS Appl. Nano Mater.* **2020**, *3*, 10234–10245.

(9) Jelley, E. E. Spectral Absorption and Fluorescence of Dyes in the Molecular State. *Nature* **1936**, 1009–1010.

(10) Scheibe, G. Über Die Veränderlichkeit Der Absorptionsspektren in Lösungen Und Die Nebenvalenzen Als Ihre Ursache. *Angew. Chemie* **1937**, *50*, 212–219.

(11) Herz, A. H. Aggregation of Sensitizing Dyes in Solution and Their Adsorption onto Silver Halides. *Adv. Colloid Interface Sci.* **1977**, *8*, 237–298.

(12) Kasha, M. Energy Transfer Mechanisms and the Molecular Exciton Model for Molecular Aggregates. *Radiat. Res.* **1963**, *20*, 55–71.

(13) Knapp, E. W. Lineshapes of Molecular Aggregates, Exchange Narrowing and Intersite Correlation. *Chem. Phys.* **1984**, *85*, 73–82.

(14) Knapp, E. W.; Scherer, P. O. J.; Fischer, S. F. On the Lineshapes of Vibronically Resolved Molecular Aggregate Spectra. Application to Pseudoisocyanin (PIC). *Chem. Phys. Lett.* **1984**, *111*, 481–486.

(15) Fidder, H.; Knoester, J.; Wiersma, D. A. Optical Properties of Disordered Molecular Aggregates: A Numerical Study Optical Dynamics of Excitons in Aggregates of a

Carbocyanine Dye Low-Temperature Dynamics of Weakly Localized Frenkel Excitons in Disordered Linear Chains Determining Exciton Coheren. *J. Chem. Phys.* **1991**, *95*, 3827–74904.

(16) Spano, F. C. The Spectral Signatures of Frenkel Polarons in H-and J-Aggregates. *Acc. Chem. Res.* **2010**, *43*, 429–439.

(17) Sorokin, A. V.; Pereverzev, N. V.; Grankina, I. I.; Yefimova, S. L.; Malyukin, Y. V. Evidence of Exciton Self-Trapping in Pseudoisocyanine J-Aggregates Formed in Layered Polymer Films. *J. Phys. Chem. C* **2015**, *119*, 27865–27873.

(18) Sorokin, A. V.; Ropakova, I. Y.; Wolter, S.; Lange, R.; Barke, I.; Speller, S.; Yefimova, S. L.; Malyukin, Y. V.; Lochbrunner, S. Exciton Dynamics and Self-Trapping of Carbocyanine J-Aggregates in Polymer Films. *J. Phys. Chem. C* **2019**, *123*, 9428–9444.

(19) Song, K. S.; Williams, R. T. *Self-Trapped Excitons*; Springer Series in Solid-State Sciences; Springer: Berlin, Heidelberg, 1996; Vol. 105.

(20) Schreiber, M.; Toyozawa, Y. Numerical Experiments on the Absorption Lineshape of the Exciton under Lattice Vibrations. III. The Urbach Rule. *J. Phys. Soc. Japan* **1982**, *51*, 1544–1550.

(21) Schubert, A.; Settels, V.; Liu, W.; Wü, F.; Meier, C.; Fink, R. F.; Schindlbeck, S.; Lochbrunner, S.; Engels, B.; Engel, V. Ultrafast Exciton Self-Trapping upon Geometry Deformation in Perylene-Based Molecular Aggregates. *J. Phys. Chem. Lett.* **2013**, *4*, 792–796.

(22) Misawa, K.; Ono, H.; Minoshima, K.; Kobayashi, T. New Fabrication Method for Highly Oriented J Aggregates Dispersed in Polymer Films. *Appl. Phys. Lett.* **1998**, *63*, 577.

(23) Matsuzawa, H.; Kobayashi, H.; Maeda, T. Spectra and Mean Association Number of Porphyrin J Aggregate. *Bull. Chem. Soc. Jpn.* **2012**, *85*, 774–785.

(24) von Berlepsch, H.; Kirstein, S.; Hania, P. R.; Pugžlys, A.; Böttcher, C. Modification of the Nanoscale Structure of the J-Aggregate of a Sulfonate-Substituted Amphiphilic Carbocyanine Dye through Incorporation of Surface-Active Additives. *J. Phys. Chem. B* **2007**, *111*, 1701–1711.

(25) Didraga, C.; Pugžlys, A.; Hania, P. R.; von Berlepsch, H.; Duppen, K.; Knoester, J. Structure, Spectroscopy, and Microscopic Model of Tubular Carbocyanine Dye Aggregates. *J. Phys. Chem. B* **2004**, *108*, 14976–14985.

(26) Pawlik, A.; Kirstein, S.; De Rossi, U.; Daehne*, S. Structural Conditions for Spontaneous Generation of Optical Activity in J-Aggregates. *J. Phys. Chem. B* **1997**, *101*, 5646–5651.

(27) Caram, J. R.; Doria, S.; Eisele, D. M.; Freyria, F. S.; Sinclair, T. S.; Rebentrost, P.; Lloyd, S.; Bawendi, M. G. Room-Temperature Micron-Scale Exciton Migration in a Stabilized Emissive Molecular Aggregate. *Nano Lett.* **2016**, *16*, 6808–6815.

(28) Eisele, D. M.; Cone, C. W.; Bloemsma, E. A.; Vlaming, S. M.; van der Kwaak, C. G. F.; Silbey, R. J.; Bawendi, M. G.; Knoester, J.; Rabe, J. P.; Vanden Bout, D. A. Utilizing Redox-Chemistry to Elucidate the Nature of Exciton Transitions in Supramolecular Dye Nanotubes. *Nat. Chem.* **2012**, *4*, 655–662.

(29) Clark, K. A.; Krueger, E. L.; Vanden Bout, D. A. Temperature-Dependent Exciton Properties of Two Cylindrical J-Aggregates. *J. Phys. Chem. C* **2014**, *118*, 24325–24334.

(30) Eisele, D. M.; Arias, D. H.; Fu, X.; Bloemsma, E. A.; Steiner, C. P.; Jensen, R. A.; Rebentrost, P.; Eisele, H.; Tokmakoff, A.; Lloyd, S.; et al. Robust Excitons Inhabit Soft Supramolecular Nanotubes. *PNAS* **2014**, E3367–E3375.

(31) Clark, K. A.; Krueger, E. L.; Vanden Bout, D. A. Direct Measurement of Energy Migration in Supramolecular Carbocyanine Dye Nanotubes. *J. Phys. Chem. Lett.* **2014**, *5*, 2274–2282.

(32) Freyria, F. S.; Cordero, J.; Caram, J. R.; Doria, S.; Dodin, A.; Chen, Y.; Willard, A. P.; Bawendi, M. G. Near-Infrared Quantum Dot Emission Enhanced by Stabilized Self-Assembled J-Aggregate Antennas. *Nano Lett.* **2017**, *17*, 7665–7674.

(33) Doria, S.; Sinclair, T. S.; Klein, N. D.; Bennett, D. I. G.; Chuang, C.; Freyria, F. S.; Steiner, C. P.; Foggi, P.; Nelson, K. A.; Cao, J.; et al. Photochemical Control of Exciton Superradiance in Light-Harvesting Nanotubes. *ACS Nano* **2018**, *12*, 4556–4564.

(34) Hinton, D. A.; Ng, J. D.; Sun, J.; Lee, S.; Saikin, S. K.; Logsdon, J.; White, D. S.; Marquard, A. N.; Cavell, A. C.; Krasecki, V. K.; et al. Mapping Forbidden Emission to Structure in Self-Assembled Organic Nanoparticles. *J. Am. Chem. Soc.* **2018**, *140*, 15827–15841.

(35) Peterson, J. J.; Krauss, T. D. Photobrightening and Photodarkening in PbS Quantum Dots. *Phys. Chem. Chem. Phys.* **2006**, *8*, 3851.

(36) Krivenkov, V.; Samokhvalov, P.; Zvaigzne, M.; Martynov, I.; Chistyakov, A.; Nabiev, I. Ligand-Mediated Photobrightening and Photodarkening of CdSe/ZnS Quantum Dot

Ensembles. *J. Phys. Chem. C* **2018**, *122*, 15761–15771.

(37) Qiao, Y.; Polzer, F.; Kirmse, H.; Kirstein, S.; Rabe, J. P. Nanohybrids from Nanotubular J-Aggregates and Transparent Silica Nanoshells. *Chem. Commun.* **2015**, *51*, 11980–11982.

(38) Chuang, C.; Bennett, D. I. G.; Caram, J. R.; Aspuru-Guzik, A.; Bawendi, M. G.; Cao, J. Generalized Kasha's Model: T-Dependent Spectroscopy Reveals Short-Range Structures of 2D Excitonic Systems. *Chem* **2019**, *5*, 3135–3150.

(39) Pandya, R.; Chen, R. Y. S.; Cheminal, A.; Thomas, T.; Thampi, A.; Tanoh, A.; Richter, J.; Shivanna, R.; Deschler, F.; Schnedermann, C.; et al. Observation of Vibronic-Coupling-Mediated Energy Transfer in Light-Harvesting Nanotubes Stabilized in a Solid-State Matrix. *J. Phys. Chem. Lett.* **2018**, *9*, 5604–5611.

(40) Malyukin, Y. V.; Sorokin, A. V.; Semynozhenko, V. P. Features of Exciton Dynamics in Molecular Nanoclusters (J-Aggregates): Exciton Self-Trapping (Review Article). *Low Temp. Phys.* **2016**, *42*, 429–440.

(41) Grynyov, R. S.; Sorokin, A. V; Guralchuk, G. Y.; Yefimova, S. L.; Borovoy, I. A.; Malyukin, Y. V. Squaraine Dye as an Exciton Trap for Cyanine J-Aggregates in a Solution. *J. Phys. Chem. C* **2008**, *112*, 20458–20462.

(42) Ng, K.; Webster, M.; Carbery, W. P.; Visaveliya, N.; Gaikwad, P.; Jang, S. J.; Kretzschmar, I.; Eisele, D. M. Frenkel Excitons in Heat-Stressed Supramolecular Nanocomposites Enabled by Tunable Cage-like Scaffolding. *Nat. Chem.* **2020**, *12*, 1157–1164.

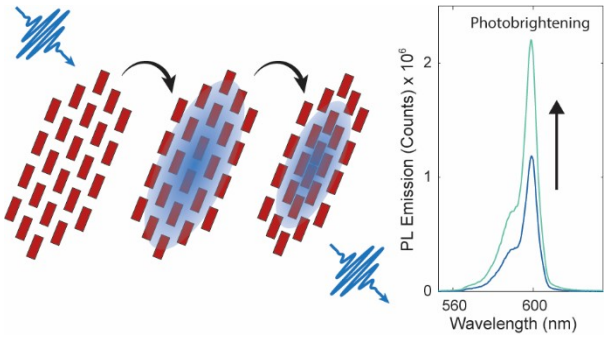
Photobrightening
PL Emission (Counts) x 10^6
2
1
0
560
600
Wavelength (nm)

TOC Graphic